STRUCTURE DETERMINATION OF QUASICRYSTALS

Marc de Boissieu, Hiroyuki Takakura, Cesar Pay Gomez, Akiji Yamamoto, a Peter Tsai

STRUCTURE DETERMINATION OF QUASICRYSTALS

Journal:	*Philosophical Magazine & Philosophical Magazine Letters*
Manuscript ID:	TPHM-06-Oct-0434.R1
Journal Selection:	Philosophical Magazine
Date Submitted by the Author:	18-Dec-2006
Complete List of Authors:	de Boissieu, Marc; LTPCM UMR CNRS 5614 Takakura, Hiroyuki; Hokkaido University, Applied Physics Pay Gomez, Cesar; Tohoku University, IMRAM Yamamoto, Akiji; NIMS, Advanced Materials Lab. Tsai, A; Tohoku University, National Institute for Materials Science
Keywords:	atomic structure, quasicrystals
Keywords (user supplied):	high dimensional crystallography, phason

Structure determination of quasicrystals

M. de BOISSIEU*[1], H. TAKAKURA[2], C. PAY GÒMEZ[3], A. YAMAMOTO[4], A.P. TSAI[3]

1- Laboratoire de Thermodynamique et Physico-Chimie Métallurgiques, UMR CNRS 5614, INPG, UJF, BP 75 38402 St Martin d'Hères Cedex (France)

2- Division of Applied Physics, Graduate School of Engineering, Hokkaido University, Sapporo 060-8628, Japan

3- Institute of Multidisciplinary Research for Advanced Materials, Tohoku University, Sendai 980-8577, Japan

4- National Institute for Materials Science, Tsukuba 305-0044, Japan

*Corresponding author. Email: Marc.de-Boissieu@ltpcm.inpg.fr

Abstract

The structure determination of quasicrystals remains a complex and challenging problem. The most fruitful approach to this problem so far, has been by the use of the high dimensional crystallography. In this paper we introduce the basic tools used in this approach and illustrate it with the case of the CdYb icosahedral phase determination. The relation between the high dimensional description and the resulting 3D structure is presented. We briefly introduce the concept of phason modes and its consequences on the diffraction pattern.

Keywords: Quasicrystal, atomic structure, phason modes

AMS Subject Classification:

1 Introduction

Aperiodic crystals are a broad class of non periodic 3D ordered structure. They are characterised by a diffraction pattern presenting sharp Bragg reflections ('essentially discrete') as a signature of long range order, but which can not be indexed by a linear combination of three integer Miller indices. Generally aperiodic crystals are grouped in three different categories: incommensurately modulated structure (the modulation being either displacive or composition like), composite structures and quasicrystals. Incommensurately modulated structures are described by an average periodic structure whose atomic positions (or chemical species) are modulated by a wave whose wavelength is incommensurate with the lattice constant of the underlying average structure. Composite structures (intergrowth or inclusion compounds) correspond to the case where two icommensurate sublattices interact. Quasicrystals, discovered by Shechtman in 1982 [1], have a diffraction pattern whose symmetry is incompatible with lattice translation symmetry, for instance the icosahedral symmetry.

As shown by de Wolff, Janner, and Janssen [2-5], aperiodic crystals are best described in a higher dimensional space, where lattice periodicity is recovered. This allows an analysis of the symmetry of the aperiodic crystal and of its diffraction pattern, and a modelling of its structure making use of the high-

dimensional periodicity. Methods and software for the structure determination of modulated and composite structures have been largely developed, so that now complex incommensurate or composite structures have their structure determined with an accuracy which is comparable with what is achieved in 'standard' 3D periodic crystallography. This is not yet the case for quasicrystals, whose structure determination remains a challenging problem. Sophisticated methods have been developed for the high dimensional description of quasicrystals, and a few refinement procedures against diffraction data have been proposed. However, a complex 'tayloring' of the model has to be developed for each case. The recent discovery of the binary CdYb icosahedral phase has been a breakthrough in that respect.

The paper is intended to give an introduction to the method used for the structure determination of quasicrystals. The principles of the method are presented on a simple 1D example in section 2 and then generalised to the case of 3D icosahedral quasicrystals. Some of the principles used to model quasicrystals are then briefly presented. The i-CdYb structure determination is presented in section 3. Finally an introduction to phason modes in quasicrystals is given in section 4.

2 Structure determination of quasicrystals: principles

2.1 A simple 1D example.

The simplest toy model for quasicrystal (QC) is the so-called Fibonacci chain. It consists of two segment lines a long (L) and a short (S) one, whose lengths are in the ratio L/S=τ, where $\tau=(1+\sqrt{5})/2=1.618\ldots$ is the golden mean. Although the non-periodic symmetry can not be dealt with in such a simple 1D example, it allows to grasp the essential features of the structure determination of quasicrystals. The Fibonacci chain can be generated by a substitution rule such as *S*->*L* and *L*->*LS*. Starting from a *S* segment the successive series are *S, L, LS, LSL, LSLLS, LSLLSLSL, LSLLSLSLLSLLS*… which at infinity give the Fibonacci chain. The diffraction pattern of the Fibonacci chain is non periodic but can be indexed by a linear combination of two wavevectors whose lengths are incommensurate. This means that the Fibonacci chain can be described in a 2 dimensional space in a periodic way. This is illustrated in figure 1 (a): the higher dimensional periodic space is a square lattice with a lattice constant *a*. It decomposes in two 1D subspaces: the parallel (or external) space which corresponds to the 1D physical space, and the perpendicular (or internal) space. The slope of the parallel space is irrational and equal to 1/τ. Each lattice node is decorated by a segment line, named atomic surface, which has an extension only in the perpendicular direction. The length of the atomic surface is obtained as the projection of the square unit cell onto the perpendicular space. The 1D Fibonacci chain is then obtained as a section of the decorated 2D periodic lattice by the 1D parallel space E_{par}. Each time the E_{par} line crosses a segment line, an atomic position is generated as shown in figure 1-a. There are several advantages in using the 2D periodic description of the Fibonacci chain. First, it is easy to carry out a statistical analysis of the different local environments in the high dimensional space. There is in fact a one to one correspondence between the generated local environments in physical space and the way the atomic surfaces are placed in the 2D periodic space. For instance it is easy to realise from Figure 1-a that the first interatomic distances in the Fibonacci chain are *S* and *L,* given by the projection of the (1,0) and (0,1) vectors onto the parallel space. As shown on the insert, all the successive generated points can be seen on the unit cell, shaded as a grey area. The successive paths of the parallel space cut are shown: starting from a point A the line goes up to B, this point is equivalent (by lattice translation) to the point B' (dashed line). From this point the cut can continue. At infinity, since the slope is irrational, the square unit cell is uniformly covered, from which one can deduce that the point density of the 1D QC is equal to D_{per}/a^2, where D_{per} is the length of the atomic surface. From this analysis one also readily realises that the frequency of the *L* segment is higher than the one of the *S* segment.

In fact, the 2D image of the Fibonacci chain can be made such as to highlight this distribution of *L* and *S* segments as shown Figure 4 (left). The decomposition into two block allows one to calculate the frequency of *L* and *S* bonds which is proportional to the ratio of each of the grey square in Fig 4 to $V_{cell}=a^2$. The second advantage of the 2D image of the quasicrystal is that it allows an easy computation of its Fourier transform. Indeed the structure is described as the convolution of a square lattice with a decoration where the decoration is a step like function, extended only in perpendicular space, with a length equal to D_{per}. Since the Fourier transform (FT) of a convolution A*B is the product of the FT(A) by FT(B), it follows that the FT of the decorated 2D square lattice is a square lattice of lattice constant $2\pi/a$, whose points have integer coordinates $Q=(n1, n2)2\pi/a$. This 2D reciprocal vectors also decomposes in two 1D reciprocal vector Q_{par} and Q_{per} the parallel (or physical space) and perpendicular reciprocal coordinates. Each lattice point of the 2D reciprocal lattice is 'weighted' by the FT of the atomic surface, which is a *sinx/x* oscillating function decaying with Q_{per}. This acts as a kind of form factor, Bragg peaks with a small Q_{per} component having a stronger intensity. The 1D diffraction pattern is then obtained as a projection of the 2D diffraction pattern onto the 1D parallel space.

(INSERT Figure 1 here)

Starting from this simple Fibonacci chain, there are a few modifications which have a strong influence onto the resulting quasiperiodic structure. The first modification, shown figure 1-b, is to increase the length of the atomic surface. As seen on the figure, this generates new atomic positions. Note that these new atomic positions can not be accounted for by a simple and systematic decoration of the L and S Fibonacci tiles. The second modification, shown figure 1-c, is to decorate the 2D square lattice with other atomic surfaces: besides the node atomic surface, two supplementary atomic surfaces have been added and are located on position (0.5,0) and (0,0.5) or mid-edges positions. As seen on the resulting 1D QC, new positions are again generated and fall at positions in the middle of the L or S segment. Finally, the atomic surfaces are not necessary 'flat' in the perpendicular directions, but can be slightly displaced along the parallel space as shown figure 1-d. This has been called a 'parallel component' of the atomic surface and results in small displacements of atoms in the resulting 1D QC, a situation which is important to 'relax' the atomic position as a function of the local environment. Such a parallel component was for instance observed by Lançon et al. [6] in relaxing a realistic i-AlMnSi model under a set of pair potential (see also [7]). Altogether we thus have shown that the high dimensional description of the QC is intimately related to the resulting 1D QC and local environments. The three important parameters describing the QC structure are thus the position of the atomic surfaces, their shape, and their parallel component. In the case of a multi component quasicrystal, the chemical content of each atomic surface needs also to be specified.

Let us now consider the structure determination problem. As an example we start from the structure of figure 1-d, shown enlarged in figure 2. Experimentally the accessible measurable quantity is the integrated intensity of the Bragg reflections, which is proportional to the square of the FT of the structure. The diffraction pattern of this 1D QC is shown figure 2 (left panel, bottom). It has been indexed with two integers which allows one to 'lift' it up in a 2D reciprocal space. At this point one is faced with the well known phase problem. When phases are unknown, the only quantity which can be computed is the Patterson function (figure 2, right panel, bottom) obtained as the FT of the measured Bragg peak intensities. Interpreting such a function is in general not obvious, but for quasicrystals it allows determining the positions of the atomic surfaces. In some cases one can also extract some rough estimate of the size of the atomic surfaces. Recently, phase reconstruction methods have been proposed by several research teams: the minimum charge density [8], the low density elimination [9] and the charge flipping method [10]. These methods might be viewed as a generalisation of direct methods (although a strict proof has not been given), with as a basis the observation that the electron density should be positive, and that the atomic surfaces are confined in limited regions in the

2D space (this corresponds to the atomicity hypothesis used for 3D direct methods). As a result it is thus possible to directly compute the electron density in the periodic space. This is of course a tremendous simplification in the structure determination of QC.

INSERT FIGURE 2 ABOUT HERE

As an example, the 2D density, as obtained by FT of the structure factors and their phases, is shown in figure 2 (right panel, top). The three atomic surfaces located on the nodes and mid-edges of the square lattice are clearly visible. It is also possible to get some insight in their length. However, when compared with the initial structure, because of the truncation effect in the FT [11], the atomic surfaces are found to be too long. This is also visible on the density profile which displays a smooth cut off, instead of a sharp one. Such a smooth profile result in 1D QC atomic positions which appear as partially occupied, and also to unphysical 'short' distances (one is encircled in the figure 2), sometime named 'split positions'. Of course here the solution should be one in which these split positions are suppressed since they do not appear in the 'real' structure. It is thus necessary to have a modelling step, with as a basis the results of the density map. This is a difficult problem which we will deal with in section 2.3.

2.2 Icosahedral quasicrystals

The previous description can be generalised to the case of icosahedral quasicrystals (see [12] for an introduction). Icosahedral symmetry is characterised by the presence of six 5-fold axes. The diffraction pattern of icosahedral QCs can be indexed by the linear combination of 6 vectors pointing along the 5-fold axis of the icosahedron. The use of 6 integer indices thus means that the QC periodicity is restored in a 6D space, which is the equivalent of the 2D space introduced in section 2.1. The 6D space decomposes into two 3D subspaces: E_{par} (the physical space, or external space) and E_{per} (or internal space). Now atomic surfaces are 3D objects. As an example, let us consider the Amman tiling or 3D Penrose tiling which is somehow the 3D-icosahedral equivalent of the Fibonacci chain. It is a 3D tiling with icosahedral symmetry, constructed with two rhombohedra: a 'fat' or prolate one and a 'thin' or oblate one (figure 3).

(INSERT FIGURE 3 ABOUT HERE)

The Amman tiling can be obtained as a section of the 6D cubic lattice whose nodes are decorated with a triacontahedron lying in E_{per}, as shown figure 3. This triacontahedron is obtained as the projection of the 6D cube onto the perpendicular direction. Of course it is not possible to visualise at once the 6D space. However, rational sections of the 6D space can provide a good insight in the structure. Figure 3 (right panel) displays a 5-fold rational section of the 6D decorated lattice. This section contains a 5-fold axis both in the parallel and perpendicular directions. The trace of the 6D cube is seen as a rectangle, with the (100000) axis corresponding to the short edge of the rectangle. The segment lines seen on this section correspond to the trace of the triacontahedron along its 5-fold axis. Again, the high dimensional space description is intimately related to the resulting 3D structure. For instance one sees that the rhombohedra edge distribution is given by the rectangle noted *b*. In fact, local order and local environments can be determined by geometrical consideration using the shape of the atomic surface. Such an analysis is beyond the scope of this paper, the main message being that there is a strong connection between the position and shape of the atomic surfaces and the local order in the resulting 3D QC.

Another useful piece of information which can be extracted from the 5-fold section, is the high symmetry position of the decoration in the 6D cube. Indeed the section contains the body centre site with coordinate 0.5(111111), noted BC on the figure, and the mide-edge (ME) site with coordinate 0.5(100000). It

turns out that all icosahedral phases known to date have atomic surfaces located on some of these special positions.

Following the analysis in section 2.1, the icosahedral structure is fully specified by the position and the shape of the atomic surfaces, with eventually their parallel component.

2.3 Modeling the structure of icosahedral QCs.

Modelling the shape of the atomic surfaces, which are 3D objects, is a complicated process. Ideally one should find a number of 'reasonable' parameters which can then be refined against diffraction data. The number of free parameters must be such that they are of the order 4 times smaller than the number of measured Bragg peak intensities. Unlike the case of incommensurate or composite structures, there is no 'standard' software procedure and each case is somehow a special one. In order to restrict the number of free parameters in the refinement a few hypotheses have been put forward which we briefly present in the following.

Of course, the first condition to be fulfilled is that the model reproduces correctly the atomic density and chemical composition observed experimentally. The second important constraint is that the resulting 3D QC structure does not have unphysical short distances. For instance, all Al alloys have Al-Al interatomic distances larger than roughly 2.3 Å. These two constraints already put severe limitations on the shape of the atomic surfaces but are not sufficient.

Constraints on the possible shapes of atomic surfaces have been proposed by Gratias and Katz, in trying to answer to two questions: (i) can a quasicrystal be grown from local rules. (ii) What is the constraint of the phason degree of freedom on atomic surfaces shape?

The question of the quasicrystal growth remains a fascinating problem. Understanding the way quasiperiodic long range order propagates is indeed intricate. A few models have been proposed so far, but they certainly are far from the real case. A prominent question is the one of locality: is it possible to grow a perfect quasicrystal only considering local growth rules or is there a long range mechanism that brings the information? In that respect the existence of matching rules (or local rules) has been a long standing discussion (see [13]). Local rules are in fact not growing rules: they only ensure that if a set of local environments are observed in a given structure, then the structure must be quasiperiodic. It means that the set of local environments is unique to the quasicrystal. Such local rules correspond for instance to the arrow decoration in the 2D Penrose tiling. Although local rules are not growing rules (this is easily demonstrated in the case of the 2D Penrose tiling), it is assumed that the growth of a quasicrystal with a restricted number of defects is possible using the local rules. It is certainly a necessary condition for a local growth. Katz and Gratias have shown that an icosahedral quasicrystal admits local rules, if the atomic surfaces which describe this structure are polyhedron bounded by mirror planes [14].

INSERT FIGURE 4 ABOUT HERE

The second condition is the so called 'closeness' condition, related to the phason degree of freedom of QC structures and is illustrated figure 4 in the case of the Fibonacci chain. If the parallel space is translated along the perpendicular direction, a 'new' 1D quasicrystal is generated: the new QC can not be in general superimposed on the previous one, but it has the same free energy (it is in fact 'indistinguishable'). This invariance of the free energy under a translation along the perpendicular space is associated with a phase shift in the density wave picture of the quasicrystal. In the framework of the hydrodynamic theory, this 'phase' degrees of freedom, leads to long wavelength phason modes. The effect of the E_{par} translation is illustrated

figure 4 where local rearrangements have occurred, some LS sequences being transformed in SL ones and vice versa.

If the shape of the atomic surfaces is made arbitrary, (for instance if the segment line describing the Fibonacci chain is made smaller, shown in the encircled region figure 4) situations might occur for which the translation of the cut space will make an atom 'disappear' and 're-appear' far away from its initial position. Such a situation is unphysical and/or might be too unfavourable from the energy point of view. Katz and Gratias proposed that the shape of the atomic surfaces should be such, that when displayed in the high dimensional space their surfaces should be 'connected' by planes parallel to the parallel space (shown as light grey line in the case of the Fibonacci chain figure 4, left panel): this will ensure that the physical space may slide, i.e. that any translation of this space creates energetically easy jump sites. The closeness condition is fulfilled for tilings such as the 3D Penrose one for instance.

With such constraints in mind Katz and Gratias proposed a set of polyhedra which should be used for icosahedral QC modelling [14]. Note however that combining closeness condition and chemical decoration is somehow extremely difficult to fulfil, so that in general models only consider the closeness condition for the external part of the atomic surfaces.

Another fruitful approach has been the comparison with a so-called rational periodic approximant. Indeed, if the slope of the parallel space is made rational instead of irrational, the resulting structure is periodic. In fact the golden mean number τ can be approximated by its successive rational approximants 1/1, 2/1, 3/2 …, which leads to crystal approximant with a larger and larger unit cell (figure 4, right panel). Each rational approximant has a local order which is similar (although not identical) to the one found in the quasicrystal. For instance (figure 4), the 1/1 approximant to the Fibonacci chain is a periodic stacking of LS whereas the 2/1 approximant is a periodic tiling of LSL, both local configurations being found in the Fibonacci chain. Surprisingly, it turned out that such periodic approximants have been found experimentally in a few icosahedral systems (AlMnSi, AlLiCu, ZnMgY and more recently CdYb). Although approximants might have large unit cells, they are periodic and standard methods of crystallography can be used for their structure determination. Having analysed their local environment, generally in terms of atomic cluster packing, this knowledge can be used for QC modelling. This approach has been for instance used for the first models in the i-AlMnSi [15, 16] and i-AlLiCu phases [17] . One can then try to find a quasiperiodic model that will for instance connect the clusters in the same way and maximise the cluster density. This approach will be illustrated in section 3 for the i-CdYb structure determination.

INSERT FIGURE 5 ABOUT HERE

The application of such a general scheme is shown on figure 5-a, which displays the decomposition of one of the atomic surface used by Gratias et al. for modelling the i-AlPdMn and i-AlCuFe phase[18, 19]. The atomic surfaces have been designed in such a way that the number of local environments and in particular the cluster chemical decorations are minimised. In this case no adjustable parameter is used. An approach, closer to what is achieved in regular crystallography has been proposed by Yamamoto and is displayed on the figure 5-b. This figure shows an atomic surface for the i-AlPdMn quasicrystal, in the asymmetric unit so has to highlight its interior (this atomic surface is similar to the one of Fig 5-a). As can be seen, the large atomic surface is decomposed in small subdomains. To each subdomain is assigned a set of parameters: chemical composition (Al, Pd, Mn or chemical disorder), a thermal parameter and a parallel shift. It turned out that this parallel shift is a crucial parameter for achieving a good fit [20], as already pointed out in early i-AlMnSi structure determination [21].

3. Structure determination of the CdYb quasicrystal

The recent discovery of the i-$Cd_{5.7}Yb$ [22] icosahedral phase has been a breakthrough for quasicrystal structure determination. Indeed this is the first stable binary quasicrystal, with a high structural quality (i.e. sharp Bragg reflections) and a very good Cd/Yb X-ray contrast (Z_{Cd}=48, Z_{Yb}=70). Moreover in the same CdYb system and for very similar chemical compositions the 1/1 Cd_6Yb [23, 24] and 2/1 $Cd_{5.8}Yb$ cubic periodic approximants can be synthesised. The structure of these two phases has been solved, and can serve as a basis for the parent QC structure determination [23, 24].

3.1 Atomic structure of the 1/1 and 2/1 approximant.

The 1/1 and 2/1 cubic approximants have a lattice parameter equal to 15.7 Å and 25.3 Å (equal to τ_x15.7) respectively. Both phases can be described as a packing of a large atomic cluster. This cluster is neither of a Mackay type (as observed in i-AlPdMn phases), nor a Bergman type (as observed in the Frank-Kasper quasicrystals such as AlLiCu) but shows a new arrangement of shells (figure 6). Starting from the cluster centre one finds: a Cd tetrahedron which appears in different orientations (disordered site), a Cd dodecahedron (20 atoms, R=4.6 Å), an Yb icosahedron (12 atoms, R=5.6 Å), a Cd icosidodecahedron (30 atoms, R=6.5 Å) and finally a large triacontahedron (92 atoms, R=7.6 Å) with atoms sitting on the vertices and mid-edges. This large cluster contains 158 atoms. One should note that there is no Cd/Yb disorder as a result of a size effect on one hand (Yb being a larger atom than Cd) and of Cd/Yb hybridisation effect on the other hand, as shown by ab-initio calculations of the electronic structure of the 1/1 approximant [25]. Besides the central tetrahedron, which is disordered, a few atomic positions on the triacontahedron also present some partial occupancy.

INSERT FIGURE 6 ABOUT HERE

The large triacontahedron (TRH in the following), is packed on a BCC lattice in the 1/1 approximant. The TRH are linked along the 2-fold axis (b-bond, 15.7 Å) by sharing a face and along the 3-fold axis (c-bond, 13.6 Å) where the two TRH interpenetrate and define an oblate rhombohedron (OR). The entire 1/1 structure is described by the packing of interpenetrating TRH (figure 6). The 2/1 approximant is also a packing of the TRH, having b- and c- bounds. However, there is a new interstitial cell defined by a decorated prolate rhombohedron (PR), with atoms on the vertices, along the edges and 2 atoms along the body diagonal (figure 6). This new cell is in fact a double Friauf polyhedron, a local environment which is characteristic of Frank-Kasper type structures. As expected, one finds that the 1/1 and 2/1 approximant have a similar local structure, with the noticeable exception of the PR. This is because the 'coordination' of the TRH cluster is different in the two approximants, with 6 b-bonds and 8 b-bonds in the 1/1 approximant, whereas in the 2/1 approximant there are 6 b- bonds and 7 c-bonds. Note that the clusters are significantly distorted along the 3-fold c-bonds, and do not display a perfect icosahedral symmetry. This is for instance visible on the figure 6, where the triangular faces of the icosidodecahedron are not identical. Similarly, atoms on the large TRH shells are displaced from their 'ideal position', with 3-fold vertices atoms 'pulled' away from their ideal position, whereas the neighbouring mid-edges Cd atoms are 'pushed' inside the cluster.

The large TRH cluster is thus a key building block of the structure, which as shown in the following, is also present in the QC structure. The crystal structure analysis, will serve as a basis for the QC structure modelling, with a large TRH connected along b- and c-bonds and two supplementary building blocks, the OR and the PR, which fills remaining spaces.

3.2 i-$Cd_{5.7}Yb$ 6D structure determination.

In order to analyze the structure of the i-$YbCd_{5.7}$ phase a data collection using synchrotron X-ray diffraction has been carried out on the D2AM beam line at the ESRF. A single grain of the i-YbCd phase, with a cubic size of approximately 0.3 mm, was extracted from an ingot slowly cooled from the liquid. It was sealed under inert gas in a glass capillary to avoid oxidation. The incoming X-ray energy was selected by a double Si111 monochromator and set to 20.6 keV to minimize absorption corrections. The single grain was found to be of very high structural quality, with a narrow mosaic spread of 0.03 °. Over five thousands unique Bragg reflections, with a large dynamical range of 8 orders of magnitude in intensity have been collected. The measured integrated intensities have been corrected for absorption. The data set contains a large number of reflections having a large Q_{perp} component of their wave vector; those reflections are particularly sensitive to the details of the structure and are important for any comparison with a model. The space group was determined to be Pm35 with an icosahedral lattice constant a = 0.5689 nm.

In the first step, a phase reconstruction for Fourier synthesis was achieved by applying the low density elimination method. The obtained phases and Fourier amplitudes were used to generate the electron densities within the 6D unit cell of the QC [26]. The figure 7 shows different rational sections of the 6D electron density. Figure 7-a displays the rational section of the electron density map in a plane containing a 5-fold axis both in the parallel and perpendicular space (see section 2). As highlighted with ellipsoid, the electron density maxima are located at three special positions of the 6D unit cell: at the origin (O), mid-edge (ME) and body-centre (BC) sites. Moreover, it is also observed that the electron density is higher on the BC sites, which indicates that this atomic surface represents Yb atoms, since Z_{Cd}=48 and Z_{Yb}=70. From the different sections it is also possible to identify which clusters are generated in the 3D QC. This is achieved starting from the BC site, whose atomic surface is 'empty' (no electron density) in its centre. Considering figure 7-a, the two double arrows point to two Yb atomic surfaces at a distance of 5.6 Å. This configuration is such that each time the cut by parallel space goes through the 'empty' centre, two Yb atoms are generated along the 5-fold axis at a distance 5.6 Å from the centre. This in fact corresponds to the generation of the Yb icosahedron. A similar reasoning on figure 7-b, which displays a section containing a 3-fold axis both in parallel and perpendicular space, demonstrates that around the 6D BC site, a Cd dodecahedron with a radius of 4.2 Å is generated. Note that in this case the atomic surface displays a significant parallel space component. Finally the 2-fold section (figure 7-c), demonstrates that an icosidodecahedron, with a radius 6.5 Å is also generated. A further study also shows that the large TRH is generated. We have thus from these density maps three important pieces of information: the location of the atomic surfaces in the 6D space, the rough size and chemical composition of each of the three atomic surfaces and finally the local order in terms of clusters, which demonstrates that the same large TRH, as observed in the crystal approximant, also exist in the QC.

INSERT FIGURE 7 ABOUT HERE.

Going further requires a detailed modelling which is achieved using the 3 building blocks found in the approximants [27]. The basic principle of the modelling is to find a quasiperiodic packing of the three building blocks, the main one being the TRH. This TRH has to be connected by the 2-fold b- and the 3-fold c-bound. The guidelines of the modelling are here the comparison with the 1/1 and 2/1 approximant crystals, together with information gained from the QC electron density maps. We first note that the size of the 'hole' in the centre of the BC atomic surface (fig 7-a and 7-b) is in fact very close to the one of the atomic surface which generates the so-called 12-fold sphere packing. The 12-fold sphere packing is a subset of vertices of the 3D Amman tiling which forms a network connected by only b- and c-bonds, as shown by Henley [28]. The shape of this atomic surface is a τ^2 deflated 'standard' triacontahedron, truncated along the 5-fold axis and is shown in figure 8-f , together with its trace (thick grey bar) on the figure 7-a. It is thus used to generate the

large TRH centres, insuring their proper connectivity. The further atomic shells of the large TRH can then be generated by copying this atomic surface after the appropriate translations has been applied in perpendicular space (a similar procedure was used to model the i-AlMnSi phase [29, 30]). Because the large TRH interpenetrate along the 3-fold c-bond, some translated atomic surfaces also interpenetrate as shown on the figure 8. There is moreover some free space in between some of the TRH: it can be shown that this space can be filled with oblate and prolate rhombohedra. A reasonable assumption is to decorate the OR and PR similarly to what has been determined in the approximant. Moreover, the prolate decoration is also what is found in the Laves Cd_2Yb phase. The corresponding 'supplementary' atomic surfaces fill the 'gaps' on the node and body-centre atomic surfaces, and generates the mid-edge one. The resulting atomic surfaces are shown figure 8, the label numbers corresponding to the different local environments generated in the resulting 3D quasicrystal.

Coming back to the discussion in section 2.3, the overall shape of the three atomic surfaces seems quite complex, since they are not simple polyhedra (Figure 8 a-c). Indeed the node and body centre one's are almost entirely 'built up' by the union of the same translated copy (figure 8a, b). However, the initial atomic surface (12-fold sphere packing centre) is bounded by mirror plane, and is a truncated triacontahedron (this restrict the way the triacontahedron is truncated, the Fig. 8-f shows one possibility), so that the resulting node and body-centre atomic surfaces are also bounded by 2-fold atomic planes and the necessary condition for local rules is fulfilled (note that this is only a necessary condition). The same is true for the mid-edge atomic surface, whose shape is such that it exactly 'fits' into the number 8 atomic surface, and is also bounded by mirror planes. Short distances are also prevented, except for the tetrahedral inner shell of the RTH, which is represented by a partially occupied dodecahedra (originating from atomic surfaces 2 and 7 which are not fully occupied). This is similar to what was achieved for the 1/1 and 2/1 atomic structure determination. The closeness condition is also fulfilled at different scales. Considering the cluster centres, the atomic surface 11, is fulfilling such a condition: at this scale this is the large triacontahedral cluster which 'flip' from one position to another almost equivalent one. At the atomic size, this condition is also most likely fulfilled, although a further detailed study is required to confirm this point. For instance, the mid-edge atomic surface has is part 12, which is connected to the body-centre part 8. The occurrence of significant parallel component to some of the atomic surfaces (8 and 1) is also an important point to be taken into account.

In order to achieve a comparison of the model with diffraction data, each atomic surface is then decomposed in smaller pieces. For each small piece there is a set of parameters: chemical content, Debye-Waller factor and parallel component. Altogether 251 parameters have been refined against the 5000 measured integrated intensities. The overall R-factor is equal to 9.5% which is a very good result taking into account the large number of used data [27]. The calculated density and composition is 8.88 g/cm3 and $Yb_{16.3}Cd_{83.7}$, which is in excellent agreement with the available experimental data. The result of the fit is a very ordered 6D structure: there is no Cd/Yb disorder and only a few Cd disordered sites corresponding to the tetrahedron.

3.3 Resulting 3D QC structure

Once the 6D model is refined, an analysis of the resulting 3D QC structure can be carried out, which ultimately, is used for the understanding of physical properties. QCs are complex materials and one should try to analyse their structure with various points of view and choose the one which is most appropriate for a given problem. There are three 'angles' which are interesting in considering the 3D description of the i-CdYb phase: (i) inter-connected clusters, (ii) dense atomic planes and (iii) hierarchical properties.

The description in terms of inter-connected clusters follows from the very construction of the 6D model. About 93.8 % of the atoms belong to a large TRH, which displays a very strong chemical order, with Yb atoms sitting only on the icosahedral shell. Moreover, the TRH displays distorsions along the 3-fold

connections, in a way very similar to what is observed in the 2/1 and 1/1 approximant. Locally, the icosahedral symmetry of the clusters is thus also broken in the QC, a result which somehow goes against the usual assumptions. The overall icosahedral symmetry is of course warranted by the 6D construction. The 'connectivity' of the clusters is also determined by the 12-fold sphere packing network. The average coordination number is 12 (i.e. 12 TRH are connected in average to a central one), but there are quite different environments. If the TRH connectivity is labelled by the number of b- and c- bonds (β,γ) around it (see [28]), then the most frequent arrangements are (7,5), (6,4), (7,6) and (7,7). Note that they are different from the 1/1 (6,8) and 2/1 (6,7) TRH connectivity, showing the difference in the QC medium range order.

Besides the TRH, there are also other local environments, as a result of OR and PR space filling. One interesting configuration is one in which a complete Bergman clusters is generated. Fragment of this cluster are also observed, together with a combination of PR and OR tiles. They fill the remaining space in between the TRH.

INSERT FIGURE 9 ABOUT HERE.

A description in terms of dense planes is best achieved by computing the projected electron density on a 2-fold plane as shown in figure 9. As already observed for other icosahedral quasicrystals [31, 32], the density is not at all uniform, but is concentrated and forms dense rows along particular directions. Densest planes correspond to the dense lines with the largest gaps in between them. Two set of dense planes, perpendicular to 2-fold and 5-fold directions, are highlighted on the figure. They actually correspond to the two strong Bragg reflections observed on the 2-fold and 5-fold axis. Such a description in terms of dense planes is for instance extremely useful for the study of surfaces.

Finally a description in terms of a hierarchical packing of clusters is also interesting, also not so much used right now, in particular for the interpretation of physical properties [33]. The figure 9 (right panel) displays the cluster centres in a 5-fold planes. In such a plane clusters are connected by 2-fold b-bonds shown as thick lines. Cluster centres just below and above this plane (0.25 nm apart) are also shown: they are connected along c-bonds. Starting from the centre, there is a 10-fold ring, which is the trace of an icosisodecahedron cluster of RTH. The top left insert, displays the trace of the full cluster on the 5-fold planes, with a diameter of 6.8 nm. This icosidodecahedron of TRH is highlighted in a light grey disk. This large cluster of TRH forms itself an icosidodecahedron of 'cluster of clusters', as shown by the 10 fold ring with a radius R2. This large icosidodecahedron has dimensions increased in scale by a factor τ^3, which results from the inflation properties of the 12-fold sphere packing. In this case the radius R2 is equal to $\tau^3 \times$R1. This inflation property can continue to infinity. This hierarchy most likely plays a role in the electronic and vibrational properties of QC's.

The structure of the CdYb phase is thus the first quasicrystal for which a detailed understanding of its atomic structure has been achieved and can be readily used for physical properties calculations. It can also be used as a starting point for total energy calculations based on ab-initio calculations or using adapted interatomic pair potentials. Such an approach has been applied to a canonical cell model of the i-CdYb, which has many similar points with the above 6D model [34]. Simultaneous fitting of energy and diffraction data, as proposed by Henley, Mihalkovic and Widom [35, 36] might indeed be an interesting alternative when chemical order is difficult to assign from the experimental diffraction data alone.

4. Phason modes.

Up to now we have considered the QC has being a perfect one, with a diffraction pattern consisting only of Bragg peaks modelled by delta functions. As for periodic crystals, real quasicrystals depart from this ideal model (thermal vibration, dislocations, point defects…) which induces either a Bragg peak broadening or diffuse scattering. In this section we are interested by long wavelength excitations which are present in the quasicrystals. There are of course long wavelength acoustic phonons, which lead to the well known thermal diffuse scattering (TDS). There is however a mode, specific to aperiodic crystals and named phason mode which plays a particular role and which we briefly present in the following (see [37] for a review and references therein). We already introduced phason modes when discussing the closeness condition in section 2.3. We have seen (figure 4) that it is possible to generate an infinite number of indistinguishable 1D quasicrystals by translating the parallel space cut along the perpendicular direction. This invariance of the free energy of the aperiodic crystal as the parallel space is displaced along the perpendicular direction, referred to as the 'phason' degree of freedom, has been analysed in the framework of the hydrodynamic theory of aperiodic crystals. The hydrodynamic theory predicts that new long wavelength modes, the phason modes, should appear in aperiodic crystals. The nature of the modes is however different for the different classes of aperiodic crystals. Phason modes are damped propagative modes in the case of displacive incommensurately modulated crystals, whereas they are purely diffusive modes in the case of quasicrystals. Phason modes are Goldstone like modes i.e their frequency (or the inverse of their lifetime for diffusive modes) goes to zero as their wavevector q goes to zero. This leads to a generalised elasticity theory of quasicrystals, which for icosahedral phases introduces two phason elastic constants (K1 and K2) and a phonon-phason (K3) coupling term. In the same way that thermal equilibrium phonon leads to a characteristic distribution of diffuse scattering around the Bragg reflections, long wavelength phason modes lead also to diffuse scattering. It has a characteristic shape and Q_{per} dependence, which is used in trying to evidence such phason modes by diffuse scattering measurements.

INSERT FIGURE 10 ABOUT HERE

All icosahedral phases investigated so far display diffuse scattering in their diffraction pattern whose shape and intensity distribution can be explained by the presence of phason modes in the quasicrystal. The most detailed study on phason modes has been carried out in the i-AlPdMn phase [38-41], where both room and high temperature in-situ studies of the diffuse scattering have been carried out using neutron and X-ray scattering. The experimentally observed diffuse scattering is perfectly reproduced using only 'phason' like diffuse scattering and the two K1 and K2 elastic constants. The diffuse scattering measurement alone can not indicate however if phason modes are really dynamical diffusive modes or just quenched in fluctuations. Using coherent X-ray diffraction it was possible to demonstrate in the i-AlPdMn quasicrystal that phason modes are diffusive modes for temperature larger than 500°C [42], whereas fluctuations are quenched in for temperature below 500°C.

As for other quasicrystals, the diffraction pattern of the i-CdYb phase also displays some diffuse scattering, with a shape and an intensity dependence characteristic for the presence of phason modes. This is illustrated figure 10, which shows iso-intensity contour plots of the diffuse scattering: anisotropies are markedly different from the ones due to phonon i.e. TDS. That phason modes and the associated diffuse scattering are specific for quasicrystals was demonstrated by measuring the diffuse scattering in the Zn-Sc 1/1 approximant and in the i-ZnMgSc quasicrystals [43]. These phases are isostructural to the CdYb 1/1 and i-phases. Figure 10 (right panel) displays the absolute scale diffuse intensity measured in the 1/1 ZnSc (dashed line) and the i-ZnMgSc quasicrystal (full line). There is a larger amount of diffuse scattering in the icosahedral phase than in the 1/1 approximant, the excess diffuse scattering being due to phason modes.

Having measured the diffuse scattering on an absolute scale, it is also possible to compare different phases. It has been found that the diffuse scattering intensity, roughly proportional to the inverse of the K1 phason elastic constant, is dependent on the type of icosahedral phases. For instance, the diffuse scattering intensity is roughly 5 time larger in the i-AlPdMn phase than in the i-ZnMgSc one (all other parameter being kept equal), meaning that the K1 phason elastic constant is roughly 5 time smaller in i-AlPdMn than in i-ZnMgSc. This should have some influence on their respective physical properties, although this has not yet been shown theoretically or experimentally.

Diffuse scattering due to long wavelength phason modes is thus present in all known icosahedral phases. In the i-ZnMgSc and i-CdYb phases it is not possible to conclude whether the observed phason diffuse scattering is due to dynamical or to quenched-in phason modes. By comparison with the i-AlPdMn phase, where high T dynamical studies were performed, one however does not expect phason modes to be of dynamical origin at room temperature: in this case these are most likely quenched-in fluctuations. An in-situ high temperature study would thus be of great interest in these two systems. The hydrodynamic theory is only a continuum like theory, so that the microscopical interpretation of phason modes is still an open question. It certainly originates from the long range quasiperiodic order and remains a key signature of quasiperiodicity.

5. Conclusion

We have seen that the high dimensional crystallography is a powerful tool for the structure determination of quasicrystals. It allows to taylor atomic surfaces in tight connection with local short or medium range order. The most elaborate and precise structural solution to date has been obtained in the i-CdYb binary phase. Its structure is mainly described as a quasiperiodic packing of a large triacontahedral cluster. The TRH interpenetrates along the 3-fold bonds, which largely diminishes the number of so-called ‘glue’ atoms which are found in between the TRH. The 6D modelling leads to a very detailed description of the resulting structure, with chemical order, distortion of the icosahedral clusters, dense planes and hierarchical packing of clusters. This model thus provides a unique opportunity for a detailed calculation of physical properties and for the understanding of the formation and stability of quasicrystals. Finally diffuse scattering due to longwavelength phason modes is also observed in this i-CdYb quasicrystal. Understanding its atomistic origin is certainly a key point for the understanding of the way quasiperiodic long range order propagates.

Acknowledgments: One of us (MdB) thanks S. Francoual for enlighting discussions.

Figure Captions:

Figure 1: Illustration of the 2D periodic description of 1D quasiperiodic structures. a) The Fibonacci chain. The resulting 1D QC is shown in the box below. b) A structure in which the segment lines have been made longer. New atomic positions are generated. c) A structure which is obtained as a decorated square lattice. Atomic surfaces are located on the nodes and on the mid-edges of the square lattice. d) A structure in which part of the atomic surfaces have been given a parallel component: this modifies slightly the local environments.

Figure 2: Illustration of the high dimensional structure determination. The structure together with its diffraction pattern is shown on the left panel. The right panel displays the 2D electron density (top) and the 2D Patterson function (bottom). The circled area highlights a 'split' position due to truncation effects.

Figure 3: Left panel: The prolate and oblate rhombohedra of the Aman tiling. The triacontahedron which decorates the nodes of the 6D cubic lattice is also shown. The right panel displays a rational section containing a 5-fold axis in both parallel and perpendicular space. The trace of the 6D unit cell is highlighted. The segment lines extending in the perpendicular direction are the triacontahedra traces.

Figure 4: Left: illustration of the closeness condition (see text). Right: Illustration of the relationship between the QC and successive periodic approximant.

Figure 5: (a). Chemical decomposition of one atomic surface in the i-AlPdMn phase as proposed by Quiquandon et al. [19] (b) Decomposition of the node atomic surface proposed by Yamamoto et al. in i-AlPdMn [20].

Figure 6: Top: The successive shells of the large TRH found in the 1/1 and 2/1 CdYb approximant. From left to right: Cd tetrahedron, Cd dodecahedron, Yb icosahedraon, Cd icosidodecahedron and the large triacontahedron (TRH)
Bottom: packing of the TRH in the 1/1 and 2/1 approximant together with the b- (2-fold) and c- (3-fold) bounding. The resulting three building blocks are shown in the bottom part (from left: TRH, PR and OB decorated rhomboedra)

Fig 7: Electron density map calculated by the low density elimination in the i-CdYb phase. (a), (b) and (c) are a 5-fold, 3-fold and 2-fold rational sections. In (a) the 3 atomic surfaces are encircled. The arrows in (a), (b) and (c) indicate the different atomic shells generated in the resulting 3D quasicrystal (see text).

Figure 8: External shape of the node (a), body-centre (b) and mide-edge (c) atomic surfaces of the i-CdYb 6D model (for simplicity the parallel component has been suppressed). (d) and (e) display the decomposition in the asymmetric unit of the node and body centre atomic surfaces respectively. (f) is an enlarged part of the building atomic surface. The different numbers explain which parts of the ODs generate the corresponding atomic positions in 3D physical space. The different shells of the RTH are the following: 11 generates the vacant centres of RTHs: its enlarged part is shown in (f); 2 and 7, generate the partially occupied vertex positions of the disordered Cd4 tetrahedron. 1 generates the Cd dodecahedra; 9, the Yb icosahedra; 8, the Cd icosidodecahedra; 4 and 5, the vertex positions of RTHs. 12, the mid-edge positions of RTHs. The other labels correspond to the two other building units: 3 and 13, generate the Cd positions of vertices and mid-edges of the AR and OR respectively, which are not shared with the RTHs; 10, the Yb positions inside ARs. 6, vacant centres of stellate polyhedra.

Figure 9: Left: electron density of the i-CdYb phase projected onto a 2-fold plane. Dense planes are observed perpendicularly to 2-fold and 5-fold axis. Right: Location of cluster centers in a 5-fold plane. The light grey area indicates the trace of an icosidodecahedron of TRH or 'cluster of clusters'. One slice of this 'cluster of clusters' is shown in the insert (top, left): there is a central TRH surrounded by a 10-fold ring of TRH (trace of the icosidodecahedron) and has a diameter of about 68 Å. The hierarchy and inflation is highlighted by the R1

and R2 length scale. On the outer part of the figure there is a 10-fold ring of 'cluster of clusters' analogous the 10-fold ring of TRH, but rescaled by a factor τ^3.

Figure 10: Left: Diffuse scattering measured in the i-CdYb phase. Isointensity contours have a specific anisotropy. Right: Absolute scale measurement of the diffuse scattering in the ZnSc 1/1 crystal (dashed) and in the i-ZnMgSc quasicrystal. There is an excess intensity due to longwavelenth phason in the quasicrystal.

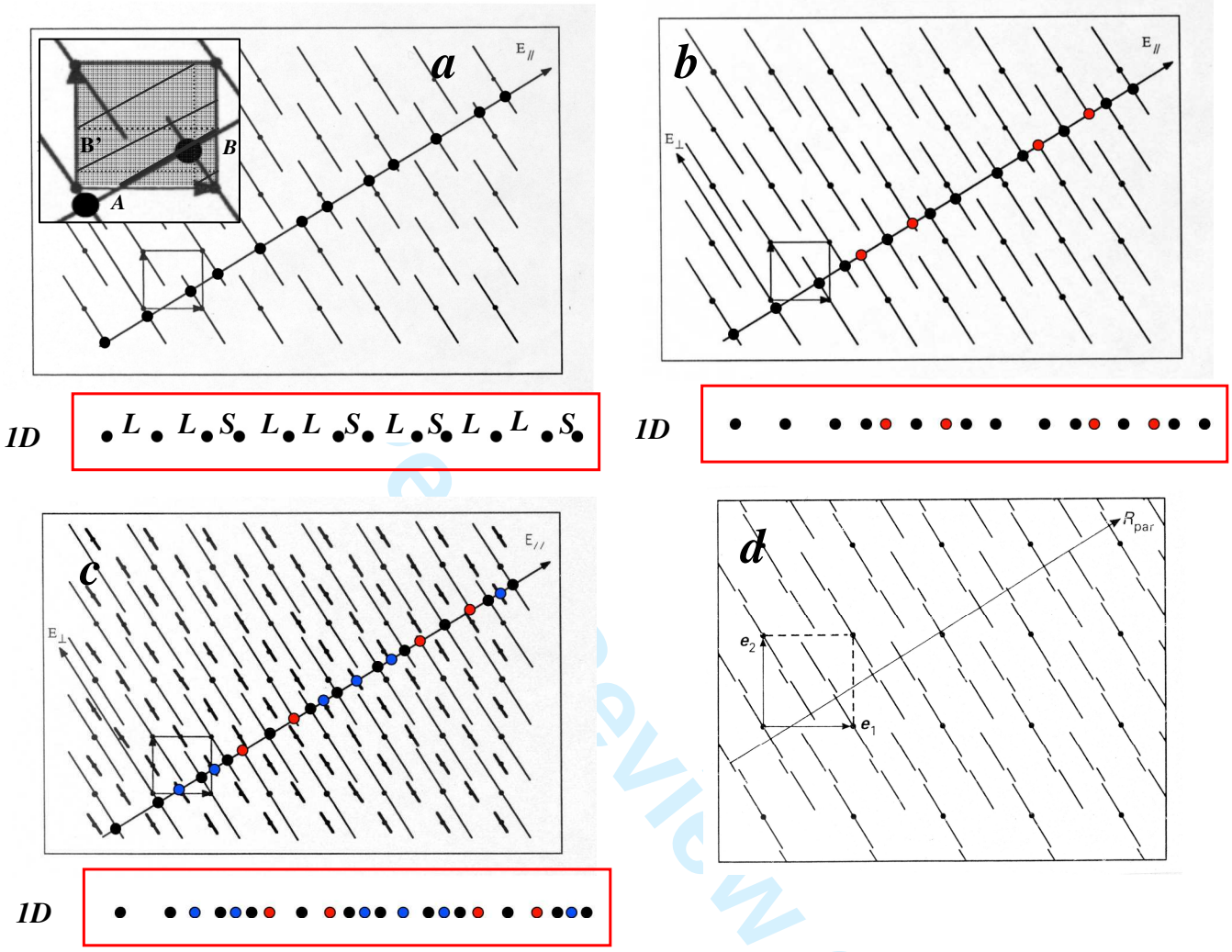

FIGURE 1

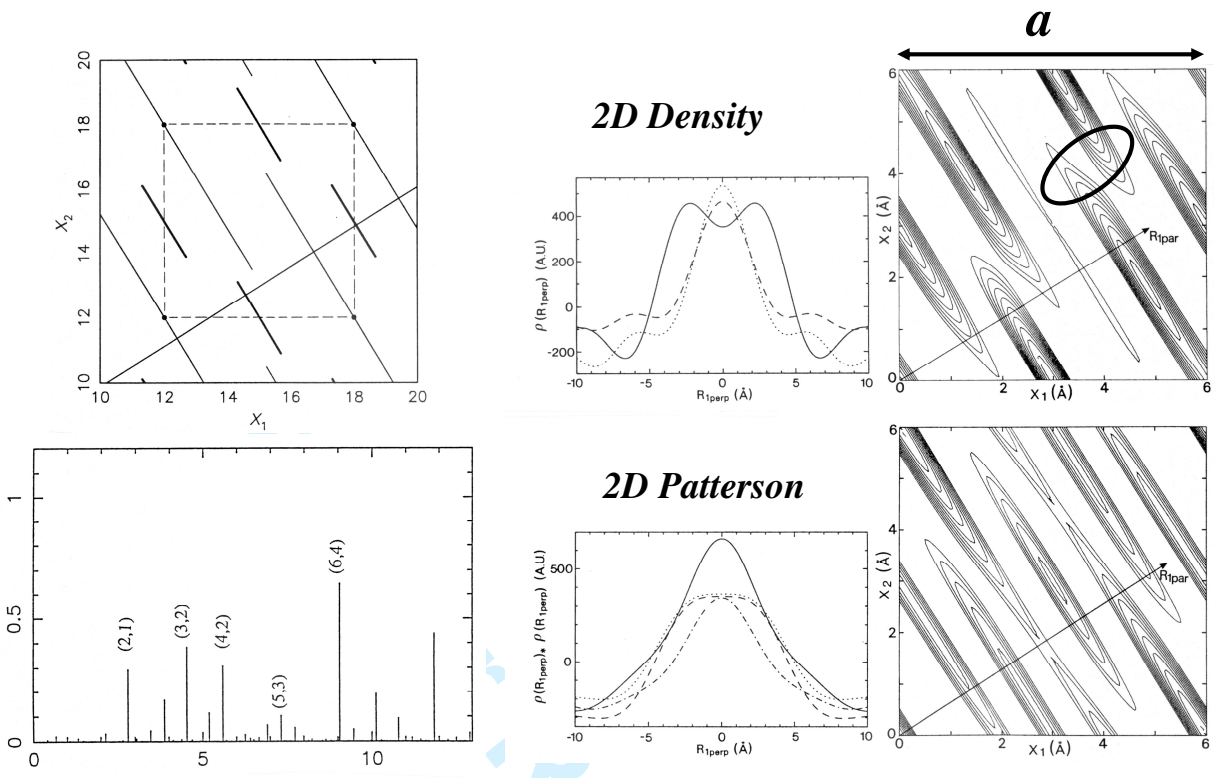

FIGURE 2

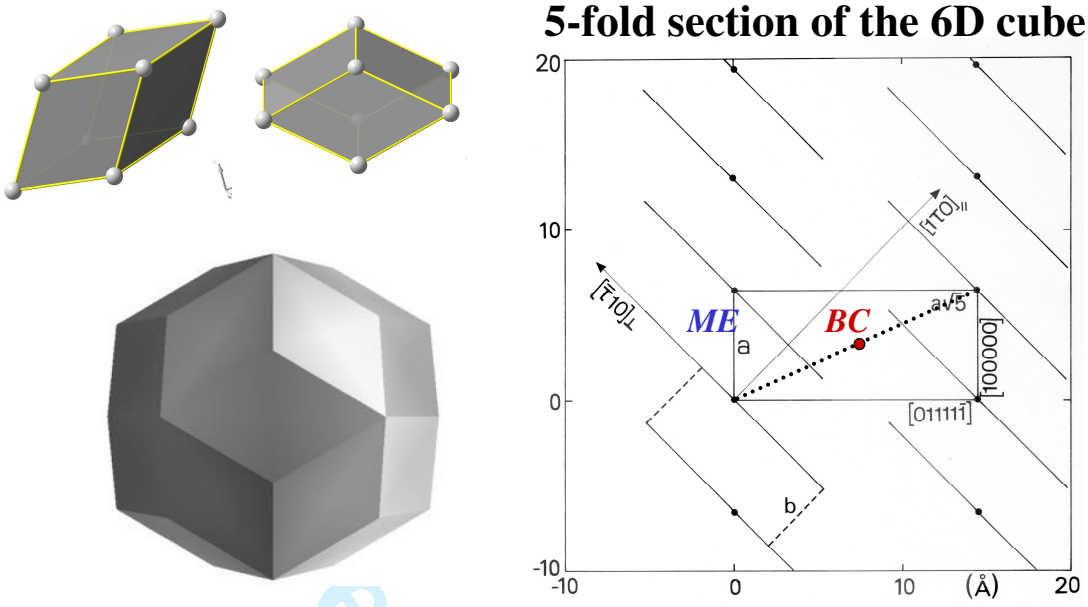

FIGURE 3

FIGURE 4

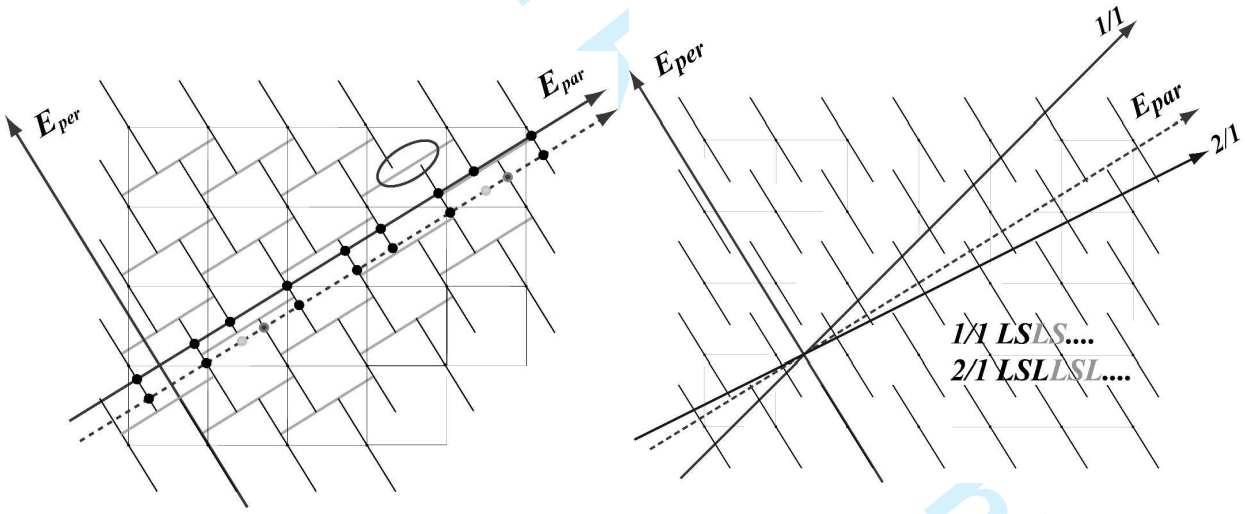

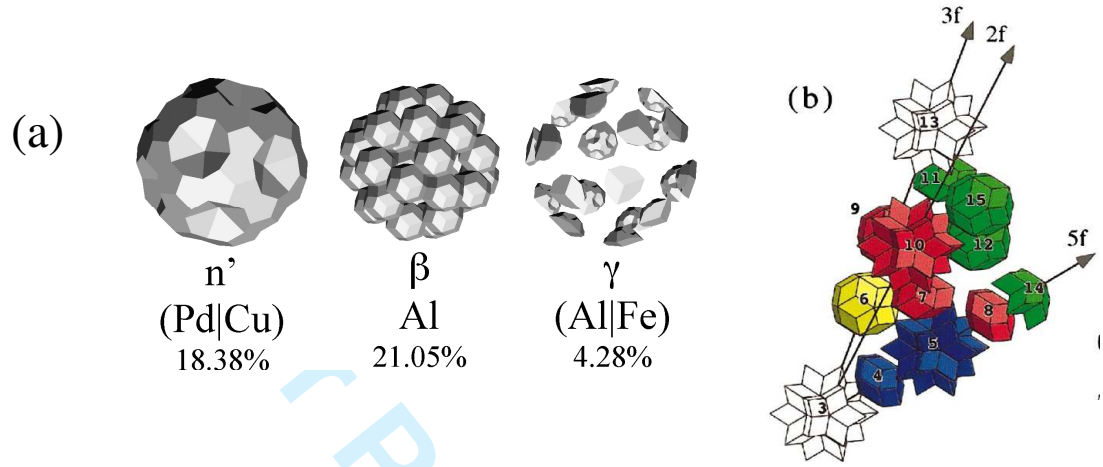

Figure 5:

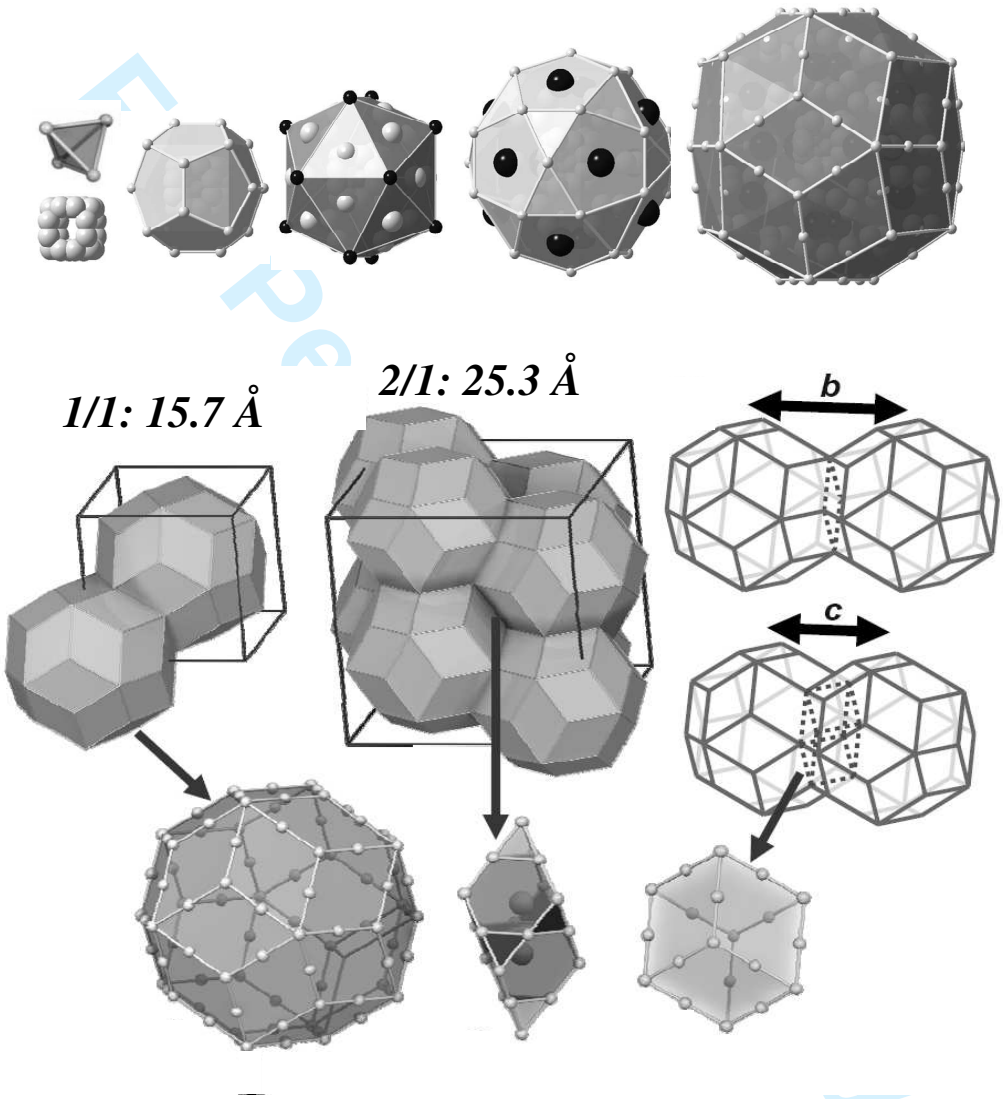

Figure 6

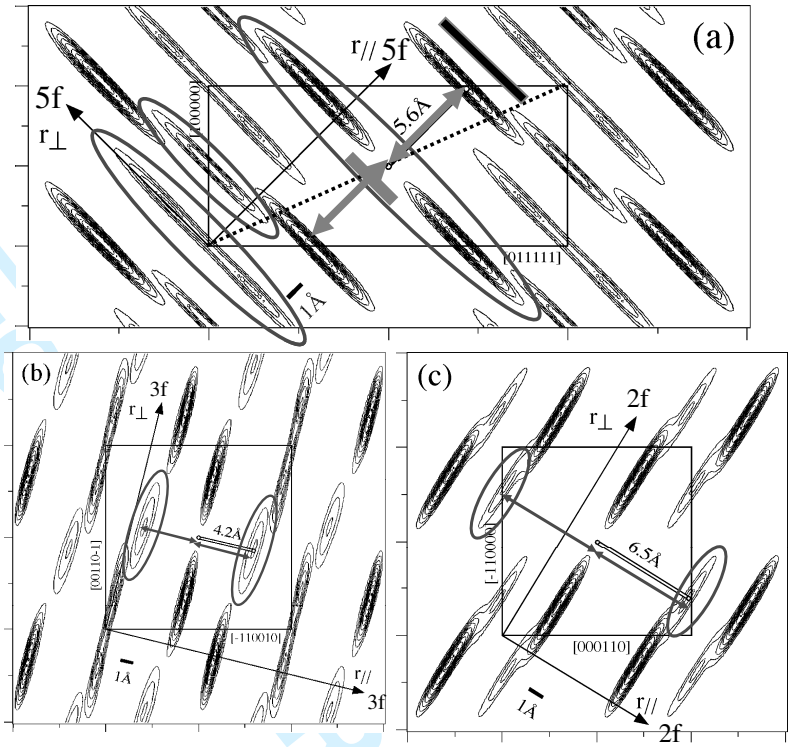

Figure 7

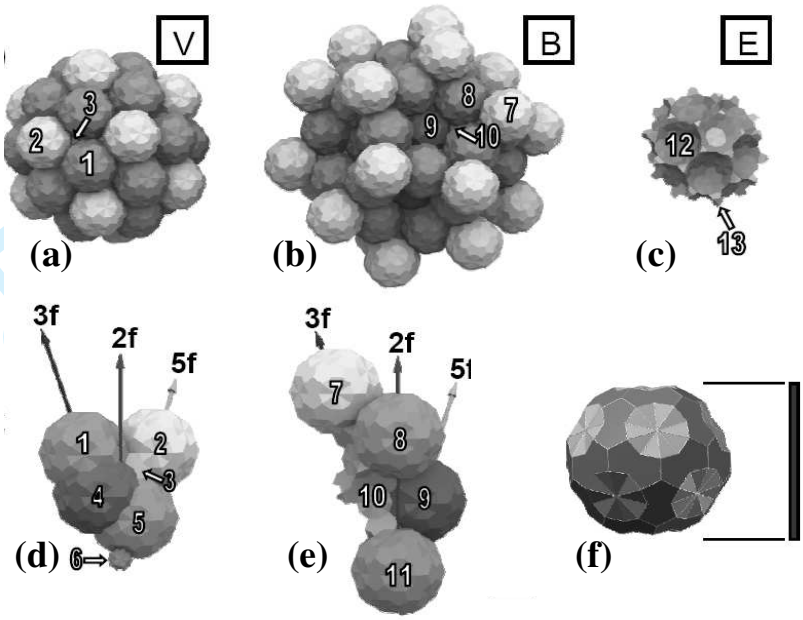

Figure 8.

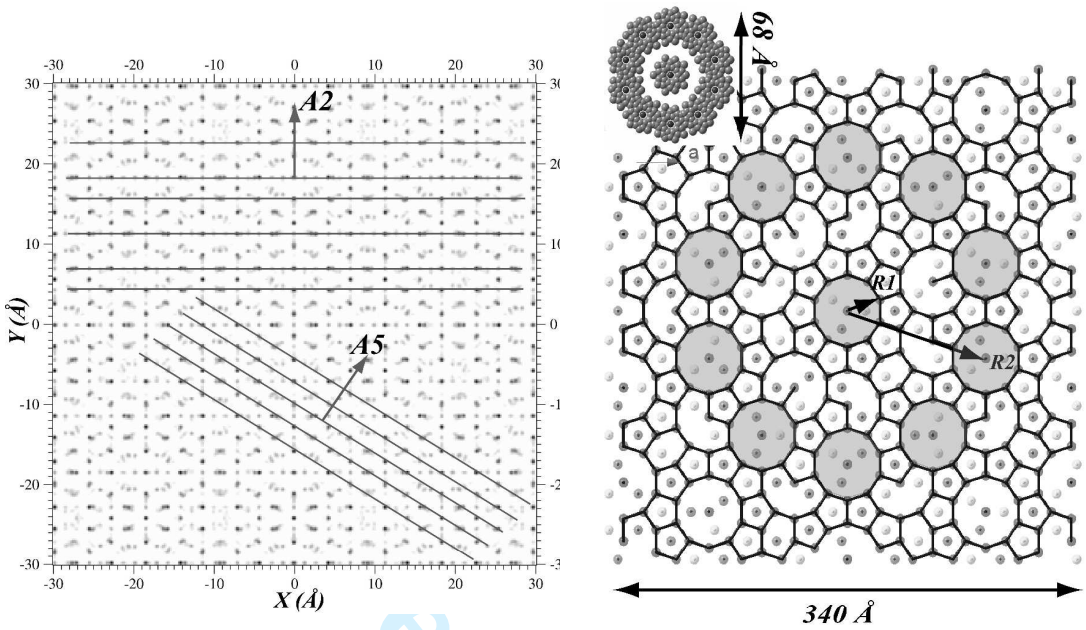

Figure 9:

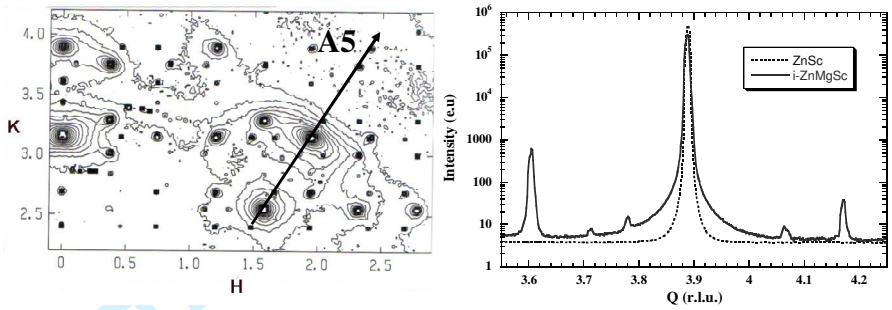

Figure 10

References

[1] D. Shechtman, I. Blech, D. Gratias and J.W. Cahn, Phys. Rev. Lett. **53** 1951 (1984).
[2] P.M. de Wolff and v. Aalst, Acta Cryst. **A28** s111 (1972).
[3] A. Janner and T. Janssen, Phys. Rev. **B15** 643 (1977).
[4] P.M. de Wolff, T. Janssen and A. Janner, Acta Cryst. A **37** 625 (1981).
[5] A. Janner, These proceedings (2006).
[6] F. Lançon and L. Billard, Journal de Physique **51** 1099 (1990).
[7] M. Mihalkovic, W.J. Zhu, C.L. Henley and R. Phillips, Phys. Rev. B **53** 9021 (1996b).
[8] V. Elser, Acta Cryst. **A55** 489 (1999).
[9] H. Takakura, M. Shiono, T.J. Sato, A. Yamamoto and A.P. Tsai, Phys. Rev. Lett. **86** 236 (2001).
[10] L. Palatinus, These proceeding (2006).
[11] M. de Boissieu, C. Janot and J.M. Dubois, Europhys. Lett. **7** 593 (1988).
[12] M. de Boissieu, P. Guyot and M. Audier, in *Lectures on Quasicrystals*, edited by F. Hippert and D. Gratias (Les éditions de physique, Aussois, 1994), p. 1.
[13] K. Ingersent, in *Quasicrystals : the State of the Art*, edited by D. P. Divincenzo and P. J. Steinhardt (World Scientific, 1991), Vol. 11, p. 185.
[14] A. Katz and D. Gratias, in *Lectures on Quasicrystals*, edited by F. Hippert and D. Gratias (Les Editions de Physique, 1994), p. 187.
[15] P. Guyot and M. Audier, Phil. Mag. B **52** L15 (1985).
[16] V. Elser and C.L. Henley, Phys. Rev. Lett. **55** 2883 (1985).
[17] C.L. Henley and V. Elser, Phil. Mag. **B 53** L59 (1986).
[18] D. Gratias, F. Puyraimond, M. Quiquandon and A. Katz, Phys. Rev. B **63** 024202/1 (2001).
[19] M. Quiquandon and D. Gratias Phys. Rev. B in press (2006).
[20] A. Yamamoto, H. Takakura and A.P. Tsai, Phys. Rev. B **68** 94201 (2003).
[21] M. de Boissieu, C. Janot and J.M. Dubois, J. Phys. : Cond. Matter **2** 2499 (1990).
[22] A.P. Tsai, J.Q. Guo, E. Abe, H. Takakura and T.J. Sato, Nature **408** 537 (2000).
[23] C.P. Gomez and S. Lidin, Angew. Chem. Int. **40** 4037 (2001).
[24] C.P. Gomez and S. Lidin, Phys. Rev. B **68** 024203\1 (2003).
[25] Y. Ishii and T. Fujiwara, J. of alloys and compounds **342** 343 (2002).
[26] H. Takakura, A. Yamamoto, M. de-Boissieu and A.P. Tsai, Ferroelectrics **305** 209 (2004).
[27] H. Takakura, C.P. Gomez, A. Yamamoto, M. de-Boissieu and A.P. Tsai, Nature Materials accepted (2006).
[28] C.L. Henley, Phys. Rev. **B 34** 797 (1986).
[29] M. Duneau and C. Oguey, J. Phys. (France) **50** 135 (1989).
[30] A. Yamamoto and K. Hiraga, Phys. Rev. B **37** 6207 (1988).
[31] M. de Boissieu, C. Janot, J.M. Dubois, M. Audier and B. Dubost, J. Phys.: Condens. Matter **3** 1 (1991).
[32] M. Boudard, M. de Boissieu, C. Janot, G. Heger, C. Beeli, H. Nissen, H. Vincent, R. Ibberson, M. Audier and J.M. Dubois, J. Phys: Cond. Matter **4** 10149 (1992).
[33] C. Janot and M. de-Boissieu, Physical Review Letters **72** 1674 (1994).
[34] M. Mihalkovic and M. Widom, Phil. Mag. **86** 519 (2006).
[35] M. Mihalkovic, I. Al-Lehyani, E. Cockayne, C.L. Henley, N. Moghadam, J.A. Moriarty, Y. Wang and M. Widom, Phys. Rev. B **65** 104205/1 (2002).
[36] M. Mihalkovic and M. Widom, Phys. Rev. Lett. **93** 095507/1 (2004).
[37] M. de Boissieu, R. Currat and S. Francoual, in *Physics of Quasicrystals*, edited by T. Fujiwara and Y. Ishii (Elsevier Science, (to be published)).

[38] M. de Boissieu, P. Stephens, M. Boudard, C. Janot, D. Chapman and M. Audier, Phys. Rev. Lett. **72(22)** 3538 (1994).
[39] M. de Boissieu and S. Francoual, Z. Kristallogr. **220** 1043 (2005).
[40] M. Boudard, M. de Boissieu, A. Létoublon, B. Hennion, R. Bellissent and C. Janot, Europhys. Lett. **33(3)** 199 (1996).
[41] A. Létoublon, M. de Boissieu, M. Boudard, L. Mancini, J. Gastaldi, B. Hennion, R. Caudron and R. Bellissent, Phil. Mag. Lett. **81** 273 (2001).
[42] S. Francoual, F. Livet, M. de Boissieu, F. Yakhou, F. Bley, A. Létoublon, R. Caudron and G. J., Phys. Rev. Lett. **91** 225501\1 (2003).
[43] M. de Boissieu, S. Francoual, Y. Kaneko and T. Ishimasa, Phys. Rev. Lett. **95** 105503\1 (2005).